Short-range thermal and structural properties of Ge nanocrystals

ARTICLE *in* NUCLEAR INSTRUMENTS AND METHODS IN PHYSICS RESEARCH SECTION B BEAM INTERACTIONS WITH MATERIALS AND ATOMS · APRIL 2007

Impact Factor: 1.12 · DOI: 10.1016/j.nimb.2006.12.115

4 AUTHORS:

Leandro Langie Araujo
Universidade Federal do Rio Grande do Sul
63 PUBLICATIONS **572** CITATIONS
SEE PROFILE

Patrick Kluth
Australian National University
139 PUBLICATIONS **1,332** CITATIONS
SEE PROFILE

Gustavo De M. Azevedo
Universidade Federal do Rio Grande do Sul
68 PUBLICATIONS **655** CITATIONS
SEE PROFILE

M.C. Ridgway
Australian National University
339 PUBLICATIONS **2,874** CITATIONS
SEE PROFILE

Available online at www.sciencedirect.com
ScienceDirect
Nuclear Instruments and Methods in Physics Research B 257 (2007) 56–59
NIM B
Beam Interactions with Materials & Atoms
www.elsevier.com/locate/nimb

Short-range thermal and structural properties of Ge nanocrystals

L.L. Araujo [a,*], P. Kluth [a], G.de M. Azevedo [b], M.C. Ridgway [a]

[a] Department of Electronic Materials Engineering, Research School of Physical Sciences and Engineering, Australian National University, Canberra, Australia
[b] Laboratório Nacional de Luz Síncrotron, Campinas, Brazil

Available online 30 December 2006

Abstract

Ge nanocrystals were produced in SiO_2 by ion implantation and thermal annealing. Size and depth distributions as well as short-range structural and thermal properties of the nanocrystals were analysed by RBS, TEM, SAXS and EXAFS. From temperature-dependent EXAFS measurements analysed using a correlated anharmonic Einstein model and thermodynamic perturbation theory it was verified that the thermal properties of Ge nanocrystals differ significantly from both bulk crystalline and amorphous Ge. For the first shell of nearest neighbours, the increase in interatomic distance with temperature for the nanocrystals was observed to be smaller than for bulk crystalline Ge. It was also observed that the first shell Ge–Ge bonds were stiffer in the nanocrystals than in both the amorphous and crystalline bulk. Such differences are ascribed to the increased surface to volume ratio of the nanocrystalline phase and the presence of the surrounding SiO_2 matrix.

PACS: 61.46.Hk; 65.80.+n; 61.72.Ww; 61.10.Ht

Keywords: Germanium; Nanocrystals; Structure; Thermal properties; Ion implantation; EXAFS

1. Introduction

Ge nanocrystals (Ge NCs) have attracted much attention in the last years due to their peculiar properties. They have proven to be promising candidates for the development of new light emitting diodes [1], flash memories [1,2], photovoltaic cells [3] and biological labelling probes [4,5]. To fully exploit their potential in such applications, a comprehensive characterization of their structural and thermal properties, both in short and long-range order, must be achieved. The short-range structural properties of Ge NCs have recently been determined [6–8] and are now briefly revisited. The short-range vibrational or thermal properties of Ge NCs are studied for the first time. Thermal properties of bulk crystalline Ge (c-Ge) have as well been investigated in this work and are compared to previous studies [9–11], reinforcing the validity of our approach. Data for amorphous Ge (a-Ge) from the literature [9,12] are presented here in order to allow an amorphous versus crystalline versus nanocrystalline phase comparison for the short-range properties of Ge. The deviations observed for such properties of the Ge NCs relative to bulk c-Ge and a-Ge reveal further differences between these states and allow us to get a deeper insight about size effects and the influence of a matrix of SiO_2 around the Ge NCs.

2. Experimental

Ion implantation of 2.0 MeV $^{74}Ge^{+1}$ ions with a fluence of 1×10^{17} cm^{-2} and at liquid nitrogen temperature, followed by thermal annealing at 1100 °C for 1 h under forming gas (N_2 95%, H_2 5%), were employed to form Ge NCs into a 2.0 μm thick SiO_2 layer grown on top of a (100) Si wafer by wet thermal oxidation. The Ge NCs were then characterized using the RBS (Rutherford backscattering), TEM (transmission electron microscopy), SAXS (small

* Corresponding author. Tel.: +61 2 612 50358; fax: +61 2 612 50511.
E-mail address: lla109@rsphysse.anu.edu.au (L.L. Araujo).

0168-583X/$ - see front matter © 2006 Elsevier B.V. All rights reserved.
doi:10.1016/j.nimb.2006.12.115

angle X-ray scattering) and EXAFS (extended X-ray absorption fine structure) techniques.

RBS measurements were performed with 3.5 MeV $^4He^{+2}$ beams. A Si surface-barrier detector was positioned at 168° relative to the impinging beam in order to collect the backscattered He ions. The resolution of the system was about 12 keV. RBS spectra were then analyzed with the aid of the RUMP program [13]. Cross-section TEM images were taken using a Philips CM300 FEI microscope with a 300 kV electron beam. The transmission SAXS measurements were carried out at beamline 15ID-D of the Advanced Photon Source, USA. A camera length of 555.4 mm and 8.27 keV X-rays (1.5 Å wavelength) were used for the measurements. Scattering images were recorded with a Bruker 6000 CCD detector at an exposure time of 5 s. Multiple images were recorded for each sample and averaged before analysis. Data were analysed based on a maximum entropy model [14]. EXAFS measurements at the Ge K-edge (11.103 keV) were performed at beam line 10–2 of the Stanford Synchrotron Radiation Laboratory, USA. Fluorescence spectra were recorded with a 30 element solid-state Ge detector and the Si (220) monochromator detuned by 50% for harmonic rejection. In order to probe the vibrational properties of c-Ge and Ge NCs, temperature-dependent EXAFS measurements from 8 to 300 K were carried out. The samples for SAXS and EXAFS analysis were prepared as described previously in [6], for example. We point out that in the preparation process the Si substrate is removed by chemical etching (KOH) so that only the SiO_2 layers containing the Ge NCs are exposed to the X-ray beams.

EXAFS spectra were energy calibrated, aligned and isolated from the raw absorbance by background subtraction via the AUTOBK algorithm, as implemented in the code ATHENA [15]. Structural parameters were then determined using ARTEMIS [15] with photoelectron momentum k and non-phase-corrected radial distance r ranges of 4.8–14.8 $Å^{-1}$ and 1.7–2.6 Å, respectively. ATHENA and ARTEMIS are GUIs (Graphical User Interfaces) for the IFEFFIT code [16]. Phases and amplitudes were calculated *ab initio* with the FEFF8.102 code [17]. The coordination number was kept constant at the bulk value of 4.0 during the c-Ge analysis and determined for the Ge NCs as 3.2 from the lowest temperature NC spectrum. It is expected to be smaller for the nanocrystalline phase due to lower-coordinated atoms at the surface. A given data set was fitted simultaneously with multiple k weightings of 1–4, in order to reduce correlations between the fitting parameters.

3. Results

The depth distribution and peak concentration of the implanted Ge atoms inside the SiO_2 layer were verified with RBS measurements. We observed a peak concentration of 3 at.% centered at a depth of 1.2 μm from the surface and with a FWHM of 0.5 μm. Comparison of as implanted and annealed samples show that there is no significant depth redistribution of Ge in the SiO_2 during the growth of the NCs, as can be seen in Fig. 1. The RBS spectrum of an unimplanted sampled is also plotted in the figure for comparison.

Crystallinity and shape of the Ge NCs were confirmed by cross-section mode TEM images. We found that the NCs are spherical in shape and present the diamond lattice structure like bulk c-Ge. A high resolution TEM image of a Ge NC is shown in Fig. 2. Due to the low contrast between the Ge NCs and the SiO_2 matrix the determination of the NCs size distribution has not been attempted from the TEM images.

Results from the SAXS measurements are shown in Fig. 3. The raw data for an unimplanted SiO_2 sample, for one sample as implanted with Ge and for one sample

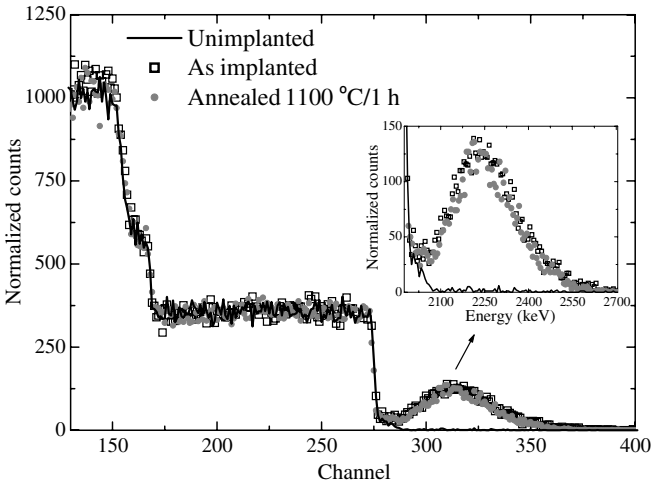

Fig. 1. RBS spectra of unimplated, as implanted with Ge and thermal annealed samples. The inset shows the Ge peaks in detail.

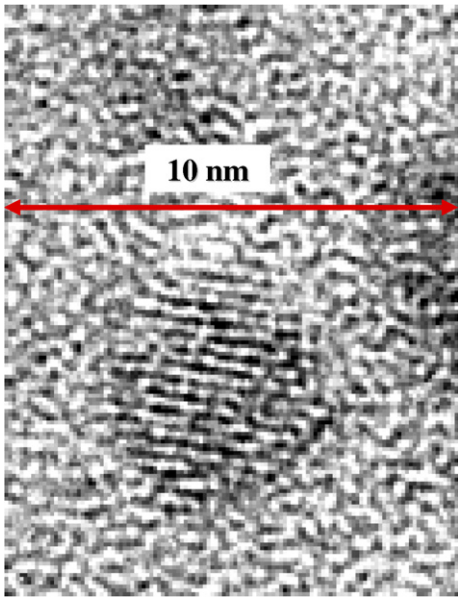

Fig. 2. HRTEM image of a Ge NC in the SiO_2 matrix.

implanted with Ge and annealed to form NCs are plotted in the figure. The inset shows the data for the NC containing sample after subtraction of the SiO_2 background (symbols) as well as the fit to the data (lines), relating to the bottom and left axes, together with the resulting volume averaged size distribution (vertical bars), relating to the top and right axes. The resulting size distribution indicates that the mean NC diameter is 4.45 nm and the FWHM is 1.50 nm. The distribution is also seen to be skewed towards higher NC sizes.

The short-range structural and thermal properties of both c-Ge and Ge NCs were obtained from EXAFS measurements in the temperature range from 8 to 300 K. Shown in Fig. 4 are the spectra acquired at 8 K for both c-Ge and Ge NCs. The EXAFS oscillations extracted from the raw data and the nearest-neighbor peaks obtained by Fourier transforming the EXAFS signals are shown in the insets. The complete thermal-dependent series of measurements and further details of the EXAFS data analysis are presented elsewhere [18]. The results obtained from the EXAFS data analysis are summarized in Table 1. For comparison, data from the literature [9,11,12] obtained through a different analysis procedure for c-Ge and a-Ge are also listed in the table. They reinforce the validity of our approach, as can be seen from the good agreement between the two c-Ge sets of results, and they also allow us to make a crystalline versus nanocrystalline versus amorphous comparison for the short-range structural and thermal properties of Ge. The structural results obtained for the Ge NCs are in good agreement with previous published results (not shown here) [6–8] if differences in the NCs mean sizes are taken into account. The structural data obtained from EXAFS are written as the cumulants [19] of the distance distribution of distances for the first nearest-neighbor shell. The first cumulant, C_1, gives the mean value of the distance distribution, which is the mean interatomic distance. The

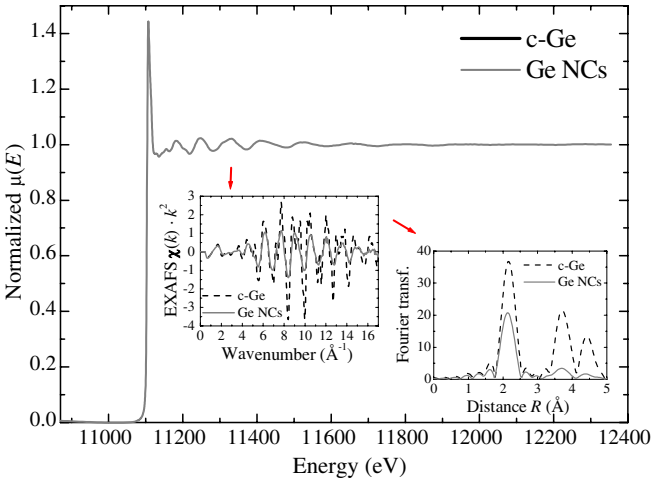

Fig. 4. EXAFS spectra obtained for c-Ge and Ge NCs at 0.8 K. The raw data are shown in the main picture, the EXAFS oscillations after subtraction of the raw absorbance are shown in the left-side inset and the Fourier transformed EXAFS presenting the nearest-neighbour shells are shown in the right-side inset.

second cumulant C_2 is related to the variance of the distance distribution and gives information about the total disorder, expressed in terms of a Debye–Waller factor. The third cumulant C_3 gives the asymmetry of the distance distribution, related to the anharmonicity of the interaction potential. The thermal variation of the cumulants can be related to an effective interaction potential between the absorber-scatterer pairs using thermodynamic perturbation theory and the anharmonic Einstein model [20]. From the temperature evolution of the first, second and third cumulants we have extracted information about the linear thermal expansion, thermal vibration (or bond strength) and asymmetry of the effective potential, respectively. It is also possible to separate the thermal and static contributions to

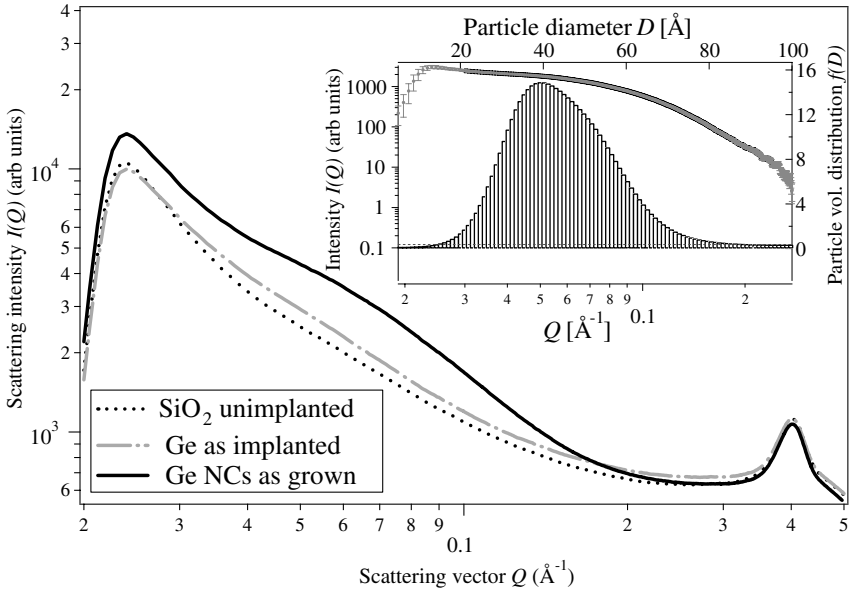

Fig. 3. SAXS spectra of unimplated, as implanted with Ge and annealed samples. The inset shows the volume averaged size distribution of the Ge NCs as grown (bars), i.e. for the annealed sample, obtained from the fit to experimental data (also shown) using the maximum entropy approach.

Table 1
Structural and thermal parameters obtained from temperature-dependent EXAFS measurements for different Ge systems

System	C_1 (Å)	C_2 (10^{-3} Å^2)	C_3 (10^{-5} Å^3)	Θ_E (K)	C_2 static (10^{-3} Å^2)
c-Ge[a]	2.450 ± 0.002	$1.92 \pm$ n.a.	0.8 ± 0.2	355.3 ± 5.7	0 (set)
c-Ge	2.452 ± 0.002	1.87 ± 0.07	0.4 ± 0.2	351.1 ± 7.2	0.02 ± 0.05
Ge NCs	2.459 ± 0.003	3.05 ± 0.17	12.5 ± 0.7	391.4 ± 11.2	1.38 ± 0.07
a-Ge[b]	2.468 ± 0.005	$4.11 \pm$ n.a.	6.7 ± 0.5	323.3 ± 4.7	2.13 ± 0.10

The first three structural parameters quoted in the table, C_1, C_2 and C_3 (mean interatomic distance, total disorder and asymmetry of the distance distribution for the first shell, respectively), are taken from the lowest temperature EXAFS data. The Einstein temperatures Θ_E and static contributions to the total disorder C_2 static are obtained from fits to the whole temperature-dependent series of EXAFS measurements.
[a] Data taken from [9,11] for comparison.
[b] Data taken from [9,12] for comparison.

the total disorder, considering that the former does not vary significantly with temperature.

The results for the total disorder (C_2 values in Table 1) show that the nanocrystals are in a state of higher configurational energy than the crystalline samples, but are not in a state as disordered as the amorphous phase. The higher static disorder (C_2 static values in Table 1) in the NCs when compared to c-Ge originates from both the reconstruction of the NCs surface due to the presence of under-coordinated atoms and the internal strain in the crystalline core [21]. The thermal contribution to the disorder, given in terms of Einstein temperatures, is higher for the NCs than both c-Ge and a-Ge, indicating that the thermal disorder grows at a slower rate for the nanocrystals and they are stiffer than the bulk phases (have stronger bond forces). Although the interatomic distance at 8 K is higher for the NC than c-Ge, its increase with temperature is slower, meaning that the linear thermal expansion is smaller for the NCs. The higher values of C_3 for the NCs show that their distance distribution is more asymmetric than for c-Ge and a-Ge even at 8 K. We assign this to the static asymmetry due to the relaxation/reconstruction of the surface atoms and the internal strain existent in the Ge NCs.

4. Conclusions

We have observed the peculiar short-range properties of a Ge NCs distribution with mean size 4.4 nm to be considerably different from the properties of both bulk phases of Ge. The NCs show stiffer bonds, lower linear thermal expansion and higher static asymmetry in their distance distribution. The higher surface-to-volume ratio of the nanocrystalline form and the presence of the SiO_2 matrix surrounding the NCs are assumed to be responsible for such differences.

Acknowledgements

L.L.A. and G. de M.A. acknowledge the Brazilian agency CNPq while P.K. and M.C.R. acknowledge the Australian Research Council and ASRP for financial support. Portions of this research were carried out at the SSRL, a national user facility operated by Stanford University, and at the Advanced Photon Source, both supported by the US Department of Energy, Office of Basic Energy Sciences.

References

[1] Z.J. Horvath, Curr. Appl. Phys. 6 (2006) 145.
[2] C.J. Park, K.H. Cho, W.C. Yang, H.Y. Cho, S.H. Choi, R.G. Elliman, J.H. Han, C. Kim, Appl. Phys. Lett. 88 (2006) 071916.
[3] H.W. Chiu, C.N. Chervin, S.M. Kauzlarich, Chem. Mater. 17 (2005) 4858.
[4] M. Bruchez, M. Moronne, P. Gin, S. Weiss, A.P. Alivisatos, Science 281 (1998) 2013.
[5] W.C.W. Chan, S.M. Nie, Science 281 (1998) 2016.
[6] A. Cheung, G.D. Azevedo, C.J. Glover, D.J. Llewellyn, R.G. Elliman, G.J. Foran, M.C. Ridgway, Appl. Phys. Lett. 84 (2004) 278.
[7] M.C. Ridgway, G.D. Azevedo, R.G. Elliman, C.J. Glover, D.J. Llewellyn, R. Miller, W. Wesch, G.J. Foran, J. Hansen, A. Nylandsted-Larsen, Phys. Rev. B 71 (2005) 094107.
[8] M.C. Ridgway, G.D. Azevedo, C.J. Glover, R.G. Elliman, D.J. Llewellyn, A. Cheung, B. Johannessen, D.A. Brett, G.J. Foran, Nucl. Instr. and Meth. B 218 (2004) 421.
[9] G. Dalba, P. Fornasini, M. Grazioli, F. Rocca, Phys. Rev. B 52 (1995) 11034.
[10] G. Dalba, P. Fornasini, R. Grisenti, J. Purans, J. Synchrotron Rad. 6 (1999) 253.
[11] G. Dalba, P. Fornasini, R. Grisenti, J. Purans, Phys. Rev. Lett. 82 (1999) 4240.
[12] G. Dalba, P. Fornasini, R. Grisenti, F. Rocca, I. Chambouleyron, C.F.O. Graeff, J. Phys.: Condens. Matter 9 (1997) 5875.
[13] L.R. Doolittle, Nucl. Instr. and Meth. B 9 (1985) 344.
[14] C.J. Gilmore, Acta Crystallogr. A 52 (1996) 561.
[15] B. Ravel, M. Newville, J. Synchrotron Rad. 12 (2005) 537.
[16] M. Newville, J. Synchrotron Rad. 8 (2001) 322.
[17] J.J. Rehr, R.C. Albers, Rev. Mod. Phys. 72 (2000) 621.
[18] L.L. Araujo, P. Kluth, G. de M. Azevedo, M.C. Ridgway, Phys. Rev. B 74 (2006) 184102.
[19] G. Bunker, Nucl. Instr. and Meth. 207 (1983) 437.
[20] A.I. Frenkel, J.J. Rehr, Phys. Rev. B 48 (1993) 585.
[21] B. Gilbert, F. Huang, H.Z. Zhang, G.A. Waychunas, J.F. Banfield, Science 305 (2004) 651.